Hindawi
Journal of Nanomaterials
Volume 2023, Article ID 2892081, 10 pages
https://doi.org/10.1155/2023/2892081

Research Article

Synthesis of Spherical Copper Oxide Nanoparticles by Chemical Precipitation Method and Investigation of Their Photocatalytic and Antibacterial Activities

Bodrun Nahar,[1] **Shakira Billah Chaity**,[2] **Md. Abdul Gafur**,[2] **and Muhammad Zamir Hossain**[1]

[1]*Department of Chemistry, Jagannath University, Dhaka 1100, Bangladesh*
[2]*Pilot Plant and Process Development Center, BCSIR, Dhaka 1205, Bangladesh*

Correspondence should be addressed to Muhammad Zamir Hossain; zamir@chem.jnu.ac.bd

Received 21 July 2022; Revised 8 December 2022; Accepted 3 February 2023; Published 20 February 2023

Academic Editor: Osman Ahmed Zelekew

Methylene blue (MB) dye and *Staphylococcus aureus* (*S. aureus*) bacteria in wastewater are the two significant problems currently. Researchers have been looking for materials that can combat these two problems at the same time. In the present study, we describe the synthesis of spherical copper oxide (CuO) nanoparticles (NPs) by the chemical precipitation method and evaluate their photocatalytic performance against MB dye and antibacterial efficacy against *S. aureus*. CuO NPs were produced using copper acetate monohydrate ($Cu(CH_3COO)_2{\cdot}H_2O$) as the precursor and sodium hydroxide (NaOH) as the reducing agent. Synthesized CuO NPs were characterized using a combination of techniques, including ultraviolet–visible spectroscopy, X-ray diffraction, transmission electron microscopy, selected area electron diffraction, Fourier transform infrared, and energy-dispersive X-ray diffraction analysis. All the analyses indicated that monoclinic CuO NPs were formed with a spherical shape and an average particle size of 6.2 nm. Photocatalytic experiments indicated that 55.5% of a 10 ppm MB dye solution was degraded by the prepared nano-CuO photocatalyst only after 60 min. Additionally, synthesized CuO NPs demonstrated, to some extent, the zone of inhibition on the *S. aureus* bacterium's cell wall. It is inspiring that CuO NPs can be used to solve two problems of MB dye contamination and *S. aureus* bacterial infection simultaneously.

1. Introduction

The main sources of water pollution include large amounts of toxic and carcinogenic dyes and bacteria, besides some other pollutants present in water, and these pollutants are mostly discharged by the pharmaceutical, cosmetics, pulp, paper, paint, rubber, and textile sectors [1]. According to a WHO report, 12 million people have died from water-borne diseases, and 10,000 tons of dyes are anticipated to be used annually in the textile sectors [2]. Numerous negative effects on human health, including kidney and liver damage, skin irradiation, narcosis, jaundice, and heat stroke, may result from the ongoing release of dyes into wastewater [3]. A literature survey indicates that dyes have a harmful effect both on the environment and human health [3]. Bacteria in water can also affect human health [4]. Because bacteria such as *Staphylococcus aureus* (*S. aureus*) are considered the parameter of water quality of drinking and bathing water [5, 6]. Again, *S. aureus* is a facultative pathogen and can be observed in several animal species as well as in the natural flora of people. They have been found on the coastal beach and river water in many regions of the world [7, 8]. Antibacterial resistance is a challenge for *S. aureus*, as well as many other bacterial disorders, particularly antibiotic-resistant diseases, which have received significant attention recently [9]. Antibacterial active agents are being researched as a workable solution.

One of the frequently used and water-polluting toxic dyes is methylene blue (MB). MB is a heterocyclic dye molecule that is long-lasting because of its complex chemical structure and is mostly used in both synthetic colors and medicines. Therefore, the effluents from the textiles, pharmaceuticals, and paper industries can contain poisonous,

cancer-causing, and persistent compounds that affect both humankind and the environment. Additionally, MB in drinking water is unhealthy since it irritates the eyes, skin, and stomach and results in hemolytic anemia, nausea, vomiting, and stomach pain. Furthermore, the developing garment industry generates tons of MB and other dye effluents, one of the leading causes of serious environmental concerns in the modern era. Therefore, it is imperative to remove MB from the water.

In this circumstance, to address the two issues described above, a nanotechnology-based material would be a worthwhile solution. Nanotechnology gained a lot of interest and played a significant role in modifying materials at the atomic and/or molecular scale because nanotechnology significantly alters the material's properties on the nanometer scale. Materials reduced in nanometer scale—nanomaterials (NMs)—exhibit substantially enhanced properties compared to what they exhibit at the macroscale or microscale. Of their special properties, NMs are being used in various applications and are being researched in new fields. Nanotechnology comprises problem identification, materials design, synthesis, and application.

Inorganic metal oxide NMs has considered for applications in dye degradation. ZnO, CeO_2, TiO_2, Fe_2O_3, etc. are well known for their photocatalytic activity [10, 11]. They have been tested for MB dye degradation and antibacterial agent. Often, composite formation and doping are also done to increase the photodegrading performance [12–14]. Recently, magnetic-MXene-based nanocomposites were also used in photodegradation [15]. Further, the photocatalytic activity of metal-based compounds was also assessed [16]. There are a good number of studies on the abovementioned metal oxides. However, research on the photodegradation of dye and combating *S. aureus* bacteria together using CuO is very limited, according to our knowledge. In this regard, therefore, evaluating the efficiency of CuO NPs would be worthwhile.

Copper oxide (CuO) nanoparticles (NPs—diameter between 1 and 100 nm) has considered for many applications. In the field of NMs, CuO is an active p-type semiconducting transition metal oxide that exhibits a narrow bandgap and has gotten a lot of attention. Because, CuO has distinct physical, chemical, and biological properties [17]. In comparison to micron-sized CuO, nano-CuO has a higher surface area per unit volume, making it superior in several applications, including antibacterial activity, dye degradation, food packaging, nanomedicine, solar cell devices, and many other fields of nanotechnology [2, 18–22].

CuO NPs can be employed as a photocatalyst as well as an antibacterial agent by dint of their distinct chemical, physical, and biological properties, as demonstrated in the previous discussion. Some papers discuss photocatalytic and antibacterial activity separately [23, 24]. However, very few reports are available that include the investigation jointly of the photocatalytic and antibacterial ability of CuO NPs. In these regards, it is crucial to select a straightforward and economical method for synthesizing CuO NPs with small sizes and narrow size distribution because size affects the catalytic activity. Various techniques, including chemical, hydrothermal, sol–gel, solvothermal, laser ablation, etc., can be used to produce CuO NPs [25–30]. Among these methods, chemical precipitation is favorable because it just needs simple tools, a precursor, and water as a cheap solvent [31–33]. CuO NP-based photodegradation is an environmentally friendly and effective method of massively reducing dye-polluted wastewater.

The current study aimed at evaluating the photocatalytic and antibacterial performance of CuO NPs. To fulfill the aim, first, CuO NPs were synthesized by the chemical precipitation method and then characterized them using various analytical techniques. Next, CuO NPs' photodegradation of MB by UV light irradiation and the disc agar diffusion method for testing CuO NPs' antibacterial activity against *S. aureus* was followed. Finally, the results were evaluated.

2. Experimental

2.1. Materials. Copper acetate monohydrate ($Cu(CH_3COO)_2{\cdot}H_2O$), purity 99%, and NaOH were purchased from Merck, Germany. Both substances were of analytical grade and were utilized directly. Oxion, a UK-based company, provided Mueller–Hilton broth (MHB) and nutrient agar for use in bacteria culture media. Merck India supplied the Muller–Hinton agar. The agar's thickness was 5 mm. The Petri dish's dimensions were 6 mm × 6 mm. Merck, India provided the MB ($C_{16}H_{18}ClN_3S$), MW 319.85 g/mol, with 95% purity. Distilled water was utilized for the experiments.

2.2. Synthesis of CuO NPs. A 100 mL aqueous solution of copper acetate monohydrate ($Cu(CH_3COO)_2{\cdot}H_2O$) at 0.1 M concentration was first made. The solution mentioned above was then vigorously stirred at 900 rpm using a DLAB (MS7-H550-S) magnetic stirrer. Next, sodium hydroxide (NaOH) aqueous solution was gradually added to it until pH turned 12. NaOH and ($Cu(CH_3COO)_2{\cdot}H_2O$) had a molar ratio of 1 : 2. The fluid turned from blue to black after 4 hr of stirring at 80°C, and the precipitate formed, indicating particle formation. During the synthesis phase, both the temperature and the stirring were maintained at a constant rate. The product was collected and washed with distilled water by centrifugation for 20 min at 10,100 rpm three times. Before characterization, the products were dried for 3 hr at 100°C.

2.3. Characterization of CuO NPs. The basic characterization of the formation of CuO NPs was carried out at room temperature using a spectrophotometer, UV-1800, Shimadzu, Japan, with a wavelength between 200 and 800 nm, and quartz cuvettes with a path length of 1 cm. Utilizing CuK radiation in a 2θ-arrangement, an X-ray diffractometer (Phillips X'Pert PRO PW 3040, Netherlands) was used to examine the crystal structure of the synthesized products. At a scanning rate of 0.02°/5 min, the range of the scanned value of 2θ angles was between 10° and 90°. For copper oxide, the measured X-ray diffraction (XRD) data and the standard XRD data from the International Centre for Diffraction Data (ICDD) card (card no. DB 01-080-1917) were compared. The shape and size of the produced CuO NPs were examined using transmission electron microscopy (TEM, TALOS F200X, 200 keV, Netherlands) with 200 kV acceleration voltages. TEM grid was prepared using dispersion droplets of CuO NPs on the copper grid. Selected area electron diffraction (SAED) technique was used to know whether

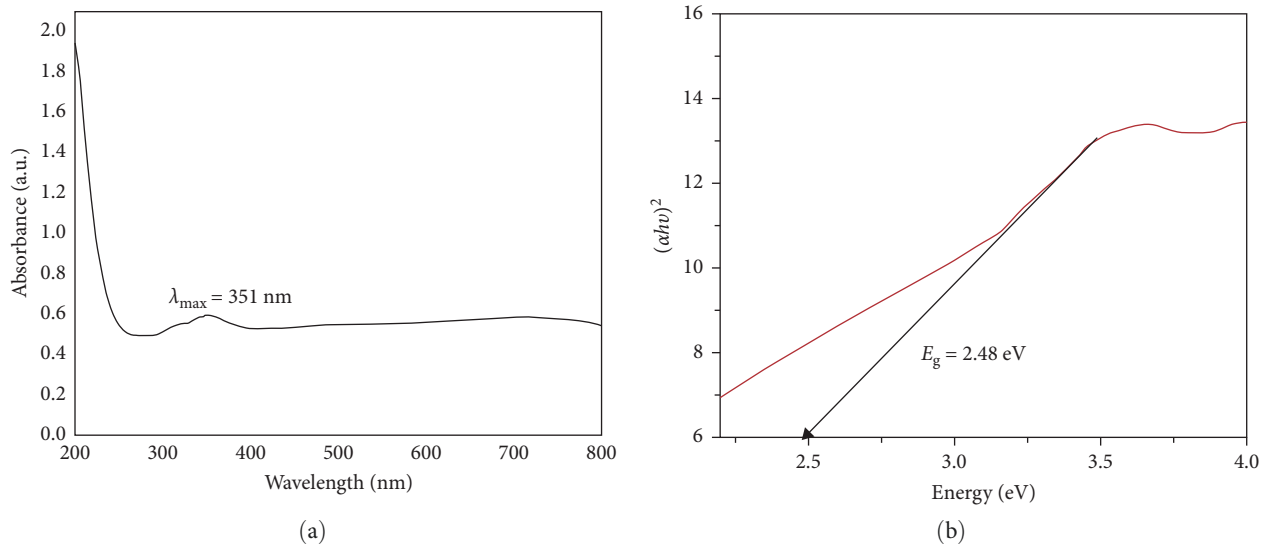

FIGURE 1: (a) UV–vis absorption spectrum and (b) bandgap energy of synthesized CuO NPs.

the product was monocrystalline or polycrystalline. Fourier transformation infrared (FTIR) spectra of the KBr pellets were obtained using a JASCO FT/IR680 spectrophotometer to investigate the potential for chemical interaction between Cu and O of the CuO NPs. An energy-dispersive X-ray spectrometer built inside the gadget was utilized to employ energy-dispersive X-ray diffraction (EDX) spectroscopy to determine the presence of components and their percentages.

2.4. Photodegradation of MB Dye. CuO NPs' photocatalytic degradation activities against MB dye were evaluated under the effect of UV light. A 50 mg of CuO photocatalyst was added to a 100 mL aqueous solution of 10 ppm MB dye. Before irradiation, the suspension dye solution was magnetically stirred for an hour in full darkness to reach adsorption–desorption equilibrium. The photocatalytic experiments were performed at ambient temperature in a beaker equipped with a magnetic stirrer and three UV tube lights with 20 W each. The distance between the UV lights and the dye solution was about 40 cm. An aluminum foil-shrouded box was used to block outside light from reaching the reaction media. The solution in the beaker was stirred at room temperature and then exposed to UV radiation. Next, 5 mL of the sample was taken for analysis of deterioration at different intervals up to 60 min. The sample was immediately centrifuged for 20 min at 10,100 rpm to remove the CuO photocatalyst. The degradation of the obtained solutions was measured from the ultraviolet–visible spectroscopy (UV–vis) absorbance spectrum obtained using a SHIMADZU UV-1800 double-beam spectrophotometer (Shimadzu Corporation, Kyoto, Japan) with a resolution of 0.5 nm and wavelength between 200 and 800 nm. Using Equation (1), the percentage of photocatalytic degradation was then determined [34].

$$\text{Percentage (\%) of photodegradation} = \frac{A_0 - A_t}{A_0} \times 100\%, \quad (1)$$

where A_0 represents the initial dye absorbance, and A_t represents the dye absorbance in the presence of CuO NPs at time t.

2.5. Antibacterial Test. The modified disk agar diffusion method, first developed by Bauer, is used for susceptibility testing [35]. *S. aureus* (ATCC 27853), the bacterial strain, was subculture on Mueller–Hilton agar media. To match the turbidity of the 0.5 McFarland standard (cell density = 1.5 × 104 CFU/mL), one loopful colony was chosen from a freshly cultured plate and used to inoculate 9 mL of MHB into a 37°C incubator overnight. The sample was generated at a concentration of 100 mg/L for antibacterial usage. The required quantity of CuO NPs was dispersed in the solvent to create the sample solution. Then, a micropipette was used to dispense 70 μL of the sample solution into the 6 mm × 6 mm-diameter holes that had been drilled in the agar media for the antibacterial activity test.

3. Results and Discussion

3.1. UV–vis Absorption Analysis. Primary evidence of the formation of CuO NPs was discovered by UV–vis absorption analysis. UV–vis absorption spectra can be used to determine the structural makeup of NPs. Figure 1 depicts the produced CuO NPs' UV–vis absorption spectra and bandgap energy. In Figure 1(a), absorption is plotted as a function of wavelength. An absorbance peak was seen in the UV region of wavelength. Exactly at 351 nm, a characteristic absorption peak appeared, which corresponded to the CuO NPs' absorption band reported previously [36, 37]. Observed characteristic absorption peak indicates the formation of CuO NPs. Also, calculated bandgap energy of 2.48 eV was found using a Touch plot for the produced CuO NPs, as seen in Figure 1(b). This bandgap energy is within the range of literature value [38].

3.2. XRD Analysis of CuO NPs. By using XRD analysis, the crystalline nature and phase structure of the generated CuO

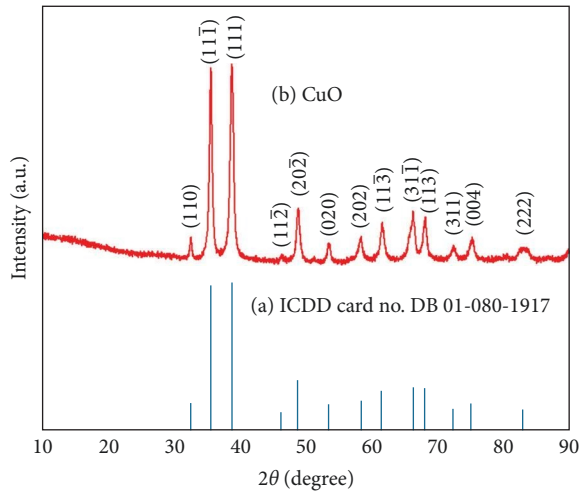

FIGURE 2: XRD pattern of (a) ICDD card no. DB 01-080-1971 and (b) synthesized CuO NPs.

NPs was confirmed. The XRD pattern of the produced CuO NPs is shown in Figure 2. A matching diffractogram in the 2θ range 10–90 with a Bragg's reflection of (110), (11$\bar{1}$), (111), (11$\bar{2}$), (20$\bar{2}$), (020), (202), (11$\bar{3}$), (31$\bar{1}$), (113), (311), (004), and (222) at 32.53, 35.57, 38.76, 46.24, 48.75, 53.43, 58.39, 61.52, 66.30, 68.13, 72.37, 75.10, and 82.95, respectively, was observed. The obtained pattern matches well with the ICDD reference of CuO (card no. DB 01-080-1917). Additionally, no impurity-related signal could be found, proving that CuO NPs were formed in a single phase [31, 39]. All the evidence proves that monoclinic CuO was formed.

It is significant to know the crystallite size of the product. Crystallite size was computed using Debye–Scherrer equation [40].

$$D = \frac{K\lambda}{\beta \cos\theta}, \tag{2}$$

where D = crystallite size, K = Scherrer constant, λ = wavelength = 1.540560 Å, β = FWHM, θ = angle (°).

The full-width half maximums (FWHM), β, of the sharpest peak is a common method used by researchers to determine the crystallite size. By doing this, it was found that the produced CuO NPs' crystallite size was 13 nm. Also, the average crystallite size was calculated from the crystallite sizes obtained from the XRD data. The calculated average crystallite size was 12.2 nm, as seen in Table 1. Also, 2θ angles, orientations, i.e., the miller indices, d-spacings, FWHMs, crystallite sizes, and average crystallite size obtained from XRD analysis of chemically synthesized CuO NPs, are shown in Table 1.

3.3. TEM Analysis. The shape and size, i.e., the surface morphology of produced NPs, were examined from TEM analysis. Figure 3(a) shows a typical TEM micrograph of chemically produced CuO NPs, demonstrating that spherical shaped particles were produced with a smooth surface. A good number of small particles with uniform shapes were seen in the micrograph. Figure 3(b) depicts the size distribution histogram of synthesized CuO NPs. Notably, a very narrow size distribution between 3 and 16 nm was achieved. To get the average particle size, the diameter of about 100 NPs was measured, and the average diameter was calculated. The calculated average diameter of CuO NPs is 6.2 nm. Additionally, the SAED micrograph (Figure 3(c)) reflected the polycrystalline structure formation of CuO NPs, which resembles the crystallite size obtained from XRD data.

We also calculated the d-spacing and intensity of signals (%) at different orientations (*hlk* planes) by analyzing the SAED pattern mentioned above and shown in Table 2. If the d-spacings obtained from SAED pattern analysis are compared with that obtained from XRD analysis, it is seen that the d-spacings of the latter are higher than that of the earlier ones. The reason for such higher values may be polycrystal formation, as seen in the SAED pattern.

3.4. FTIR Analysis. Figure 4 shows the FTIR diagram of the synthesized CuO NPs. The peaks at 506.13 and 610.66 cm^{-1} indicated the Cu–O bond formation of produced CuO NPs [41]. The abovementioned two peaks supported the monoclinic structure of CuO NPs.

3.5. EDX Analysis. Figure 5 displays the findings of an elemental composition analysis utilizing EDX spectroscopy of the generated CuO NPs. The three intense characteristic peaks for Cu at 1, 8.1, and 9 keV were observed. Another strong and sharp peak to the spectrogram is caused at 0.6 keV by oxygen. Also, a very tiny peak at 0.35 keV aroused for C that may be related to the carbon grid used to hold the sample. All the EDS data supported the synthesis of CuO NPs [42, 43].

Table 3 summarizes the data obtained from the EDX analysis, which indicates the elemental configuration. From Table 3, it is seen that the elemental ratio of Cu and O is 1 : 1, which supports the CuO formula if we avoid the atomic fraction of C, which most probably came from the carbon grid during sample analysis.

3.6. UV Light-Induced Photodegradation of MB. To assess the photocatalytic performance of synthesized CuO NPs under UV light irradiation, an aqueous MB pollutant was used. Following the dark treatment, the time track was recorded. As a control, the MB solution was leveled without the photocatalyst. By making the bulb on, the photocatalytic process was processed. Figure 6 shows the CuO NPs photocatalyst's absorption spectrum for 10 ppm MB solution as a function of wavelength. As seen from the spectrum, the intensity of peaks at 663 nm decreases gradually with the presence of catalyst and UV light irradiation. The MB solution with photocatalyst was irradiated for 60 min of UV lamp exposure, indicating that MB was degraded under light conditions. The following formula is used to calculate the rate of dye degradation [34].

$$\%\ \text{of Photodegradation rate} = \frac{A_0 - A_t}{A_0} \times 100\%, \tag{3}$$

where A_0 and A_t stand for absorbance (at 663 nm) at different times (t) and the initial dye solution, respectively.

Table 1: 2θ angles, orientations, d-spacings, FWHMs, crystallite sizes, and average crystallite size obtained from XRD analysis of chemically synthesized CuO NPs.

Angle, 2θ (°)	Orientation (*hlk*)	d-Spacing (Å)	FWHM (°)	Crystallite size (nm)	Average crystallite size (nm)
32.53	(110)	2.74989	0.3345	22.8	
35.57	$(11\bar{1})$	2.52224	0.4448	17.0	
38.76	(111)	2.32147	0.5765	13.0	
46.24	$(11\bar{2})$	1.96169	0.4046	18.1	
48.75	$(20\bar{2})$	1.86644	0.5669	12.8	
53.43	(020)	1.71340	0.5073	14.0	
58.39	(202)	1.57918	0.6746	10.3	12.2
61.52	$(11\bar{3})$	1.5061	0.6131	11.1	
66.30	$(31\bar{1})$	1.40874	0.9043	7.4	
68.13	(113)	1.37517	0.5974	11.0	
72.37	(311)	1.30472	0.7352	8.7	
75.10	(004)	1.26385	0.7382	8.5	
82.95	(222)	1.16305	1.4443	4.1	

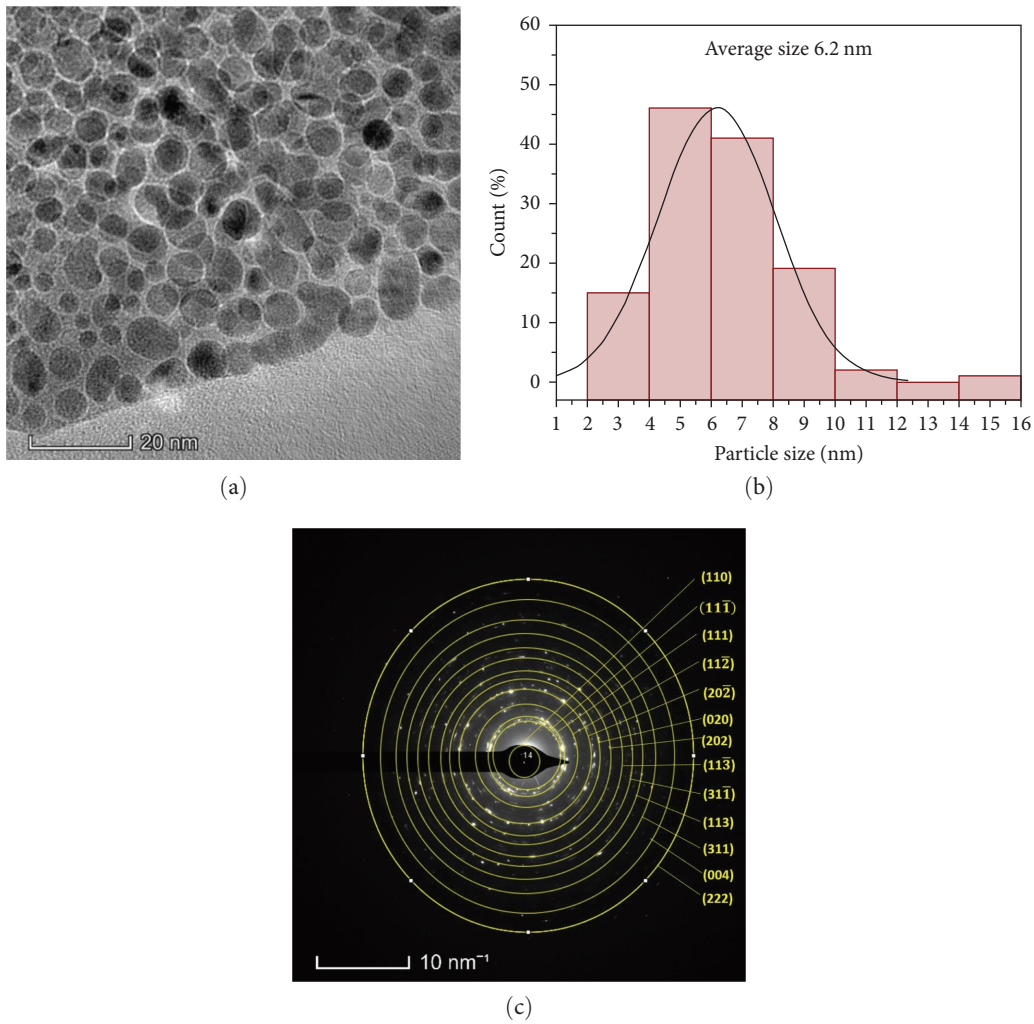

Figure 3: (a) TEM micrograph, (b) size distribution histogram of the CuO NPs obtained from TEM images, and (c) SAED pattern of CuO NPs.

According to Beer–Lambert's law, A_0 and A_t are proportional to C_0 and C_t, respectively, where C_0 represents the dye's initial concentration, and C_t represents its current concentration.

Figure 7 illustrates the efficiency of photodegradation by 60 min, which was determined to be 55.5% using Equation (1). The efficiency data from the literature (56%) is comparable to the findings of this investigation [44]. The test was performed

Table 2: Orientations and d-spacings obtained from SAED pattern analysis of chemically synthesized CuO NPs.

Orientation (*hlk*)	d-Spacing (Å)	Intensity of signal (%)
(110)	5.717553	4
$(11\bar{1})$	2.666667	79
(111)	2.295157	100
$(11\bar{2})$	1.783485	2
$(20\bar{2})$	1.363977	27
(020)	1.171852	7
(202)	1.057194	14
$(11\bar{3})$	0.924428	21
$(31\bar{1})$	0.842531	30
(113)	0.749204	20
(311)	0.671772	5
(004)	0.586734	10
(222)	0.521145	9

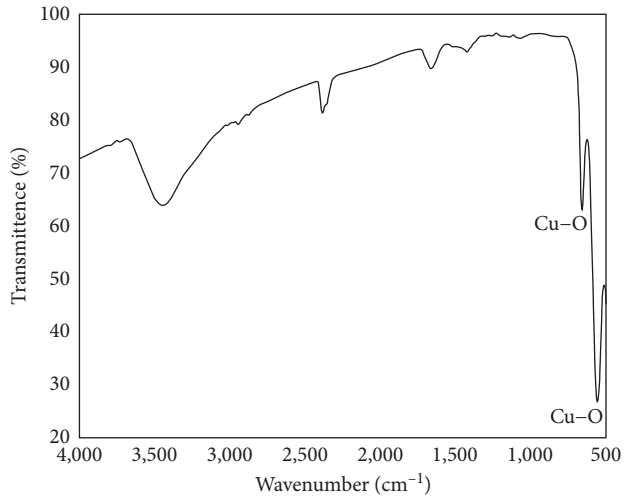

Figure 4: FTIR spectrum of the chemically synthesized CuO NPs.

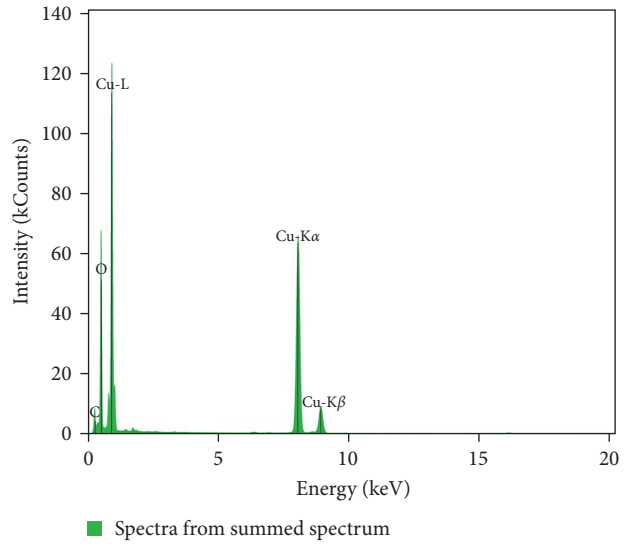

Figure 5: EDX spectrum of the synthesized CuO NPs.

Table 3: Percentage of the elemental configuration of the product.

Atomic number (*Z*)	Element	Atomic fraction	Weight fraction
8	O	47.76	20.59
29	Cu	45.02	77.08
6	C	7.22	2.34

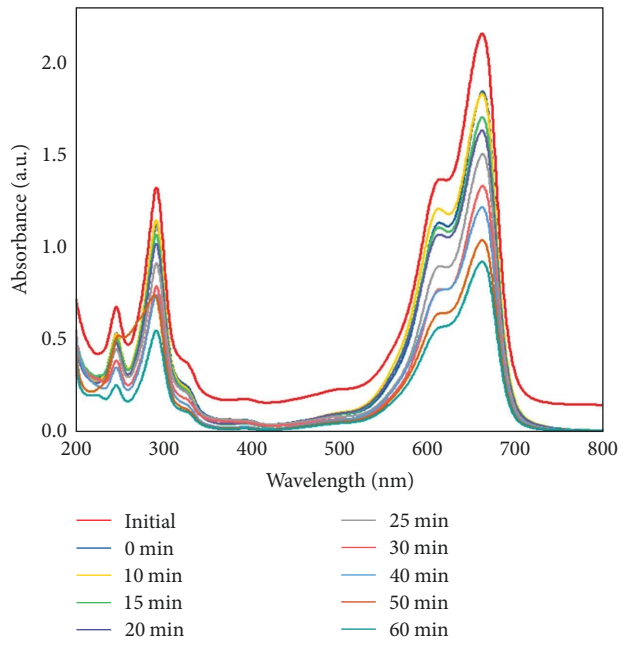

Figure 6: UV–vis spectrum of the MB photodegradation caused by the CuO NPs.

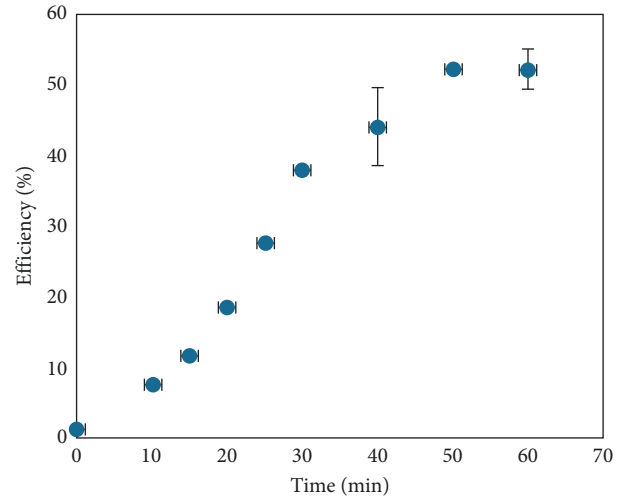

Figure 7: The efficiency calculation for the UV photodegradation of MB dye by CuO NPs.

three times, and the average values were taken to calculate the efficiency. A standard deviation error bar was added to the data of the graph. Because smaller particles have higher surface areas and a larger number of surface electrons which can

Table 4: Comparison of MB photodegradation efficiency by CuO NPs photocatalyst.

Dye (Conc.)	Type of applied light	Loading of CuO (mg)	Photodegradation efficiency (%)	Other conditions	Reference
MB (15 ppm)	Sunlight	10	34.4	3 hr, ambient temperature	[45]
MB (2.5×10^{-5} mol/L)	Sunlight	100	93	3 hr, ambient temperature	[46]
MB (5×10^{-3} M)	Sunlight	200	85	50 min	[25]
MB	Xenon lamp		52	60 min	[47]
MB (3×10^{-5} M)	Visible	20	43.5	5 hr, stirring	[44]
MB (3.13×10^{-5} M)	UV	50	81	60 min	[48]
MB (10 ppm)	UV	50	55.5	60 min, magnetic stirring	Present work

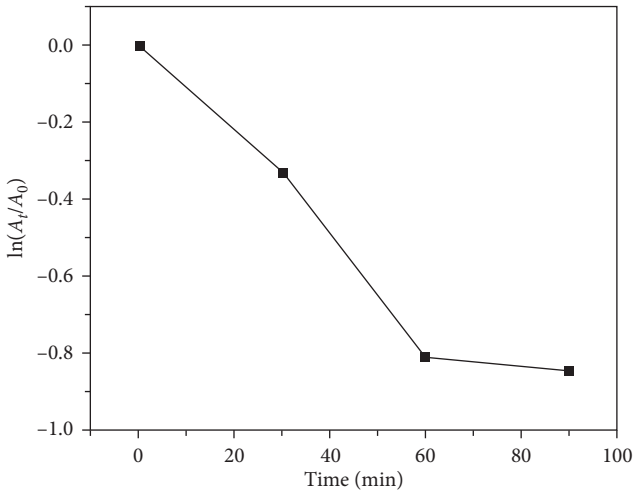

Figure 8: Kinetics analysis of MB photodegradation in the presence of UV light.

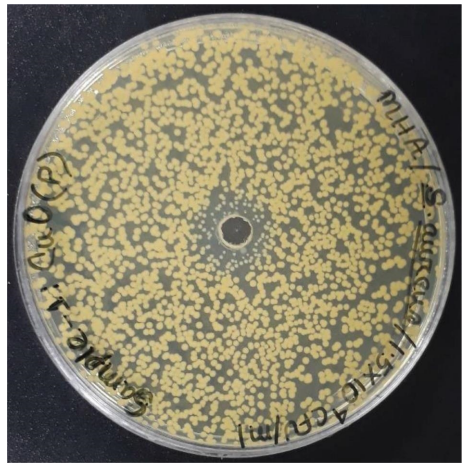

Figure 9: *S. aureus* bacterial zone of inhibition by the produced CuO NPs at a dosage of 70 μL with centration of 100 mg/L.

take part in more photocatalytic activity. Thus, the photodegradation efficiency increases.

Comparing the present photodegradation efficiency of CuO NPs with the literature data would be worthwhile. Table 4 represents the literature data and presents data on the efficiency of dye photodegradation by CuO NPs.

The relationship between the rate of dye degradation and time was calculated using the formula $\ln(A_0/A_t)$. The dye absorbance after photocatalysis and at different irradiation periods are represented by A_0/A_t, respectively. The linear fit of $\ln(A_t/A_0)$ vs. time suggested a pseudo-first-order kinetics pattern of MB photodegradation (Figure 8). The rate constant was determined to be 0.009374 min^{-1} [49, 50].

The assumed mechanism of the observed photocatalytic activity is as follows: when MB is photodegraded, CuO NPs provide the electron and the hole. When the CuO NPs are exposed to UV light with an energy equal to or greater than the bandgap, electrons (e) from the valance band (VB), and the holes (h) in the VB are transported to the conduction band (CB). CuO NPs' VB electrons will be stimulated to go to the VB, and CB will charge up as a result of the absorption of UV energy. VB and CB are split apart by a restricted band before being exposed to the light. As a result, these free e/h will try to move away from the catalyst surface and engage in interaction with the H_2O solvent and the dissolved molecular oxygen, respectively. These reactive oxygen species include hydroxyl radicals (–$OH^{\cdot}$), superoxide radicals ($O_2^{\cdot}$), hydrogen peroxide (H_2O_2), or hydroperoxyl radicals ($OOH^{\cdot}$). According to references, the MB solution would cause the photodegraded electrons to react with the dissolved O_2 molecules and produce superoxide anion radicals ($O_2^{-\cdot}$) while the holes would react with H_2O and produce hydroxyl radicals (–$OH^{\cdot}$). Both of these powerful oxidizing agents would cause the dye to degrade [25, 51].

3.7. Antibacterial Response of the Synthesized CuO NPs. Using the disc agar diffusion method, the antibacterial activity of the produced CuO NPs was assessed against *S. aureus* bacteria after an 18 hr incubation period. CuO NPs were found to have a mild inhibitory effect on *S. aureus* bacteria. The precise mechanism of antibacterial activity is unknown. However, the literature study found that pathogens perish when surface reactive metal ions are released, and metal protein complexes form on the surface of CuO NPs. At a dose of 100 mg/L, the zone of inhibition, seen in Figure 9, was calculated to be 12 mm which is comparable with the reference values [52]. The outcomes were contrasted against the widely used antibiotic amoxicillin.

Table 5: Comparison of zone inhibition of bacteria by CuO NPs photocatalyst.

Antibacterial agent	Concentration	Zone of inhibition (mm)	Reference
S. aureus	25 mg/mL	11	[45]
S. aureus	4.2 mg/mL	10.5	[45]
S. aureus	50 μg/100 mL	12	[53]
S. aureus	25 mg/mL	14	[54]
S. aureus	100 mg/L	12	Present work

The present work's zone inhibition data and literature data are presented in Table 5 for comparison.

4. Conclusions

Using the chemical precipitation method, we successfully synthesized spherical CuO NPs. Produced CuO NPs were characterized by UV–vis, XRD, TEM, SAED, FTIR, and EDX spectroscopy. The UV–vis peak at 351 nm indicated that CuO NPs were predominantly formed. The product's XRD pattern revealed that crystalline CuO was formed and had a monoclinic crystal structure. The calculated average crystallite size from XRD data was 12.2 nm. CuO NPs that were produced and had an average particle size of 6.2 nm were found to be spherical according to TEM analysis. Notably, a very narrow size distribution between 3 and 16 nm was achieved. The larger crystallite size is probably to the polycrystal structure of CuO NPs, as evidenced by the SAED pattern. The presence of Cu and O in the synthesized sample indicates the purity, which was confirmed by EDS elemental analysis. FTIR peaks at 506.13 and 610.66 cm^{-1} indicate the bond formation between Cu and O (Cu–C) of CuO NPs. Photocatalysis experiments using UV–vis spectrum analysis indicated that 55.5% of a 10 ppm MB dye solution was degraded by the prepared CuO NPs only after 60 min. The kinetics study depicts a pseudo-first-order reaction with a rate constant of 0.009374 min^{-1}. At a dosage of 100 mg/L, CuO NPs demonstrated a moderate antibacterial response against *S. aureus*, with a 12 mm zone of inhibition. This research suggests that CuO NPs can solve two problems of dye contamination and bacterial infection at a time. Present work may help further research on the photodegradation of dye and antibacterial tests with CuO NPs.

Data Availability

Corresponding author will provide data on requst.

Conflicts of Interest

The authors declare that they have no conflicts of interest.

Funding

This research was supported by a grant (no. 08/Science/2021-2022) from the Jagannath University Research Project financed by the University Grants Commission of Bangladesh.

Acknowledgments

We acknowledge the AIC, Jagannath University, PP & PDC, BCSIR, Atomic Energy Centre, Dhaka and Waffen Research Lab, Dhaka for analytical support.

References

[1] G. Vijayakumar, H. Kesavan, A. Kannan et al., "Phytosynthesis of copper nanoparticles using extracts of spices and their antibacterial properties," *Processes*, vol. 9, no. 8, Article ID 1341, 2021.

[2] S. Vasantharaj, P. Shivakumar, S. Sathiyavimal et al., "Antibacterial activity and photocatalytic dye degradation of copper oxide nanoparticles (CuONPs) using *Justicia gendarussa*," *Applied Nanoscience*, 2021.

[3] B. Lellis, C. Z. Fávaro-Polonio, J. A. Pamphile, and J. C. Polonio, "Effects of textile dyes on health and the environment and bioremediation potential of living organisms," *Biotechnology Research and Innovation*, vol. 3, no. 2, pp. 275–290, 2019.

[4] S. Das, N. Ranjana, A. J. Misra et al., "Disinfection of the water borne pathogens *Escherichia coli* and *Staphylococcus aureus* by solar photocatalysis using sonochemically synthesized reusable Ag@ZnO core–shell nanoparticles," *International Journal of Environmental Research and Public Health*, vol. 14, no. 7, Article ID 747, 2017.

[5] N. Topić, A. Cenov, S. Jozić et al., "*Staphylococcus aureus*—an additional parameter of bathing water quality for crowded urban beaches," *International Journal of Environmental Research and Public Health*, vol. 18, no. 10, Article ID 5234, 2021.

[6] F. M. Schets, H. H. J. L. van den Berg, G. Lynch, S. de Rijk, A. M. de Roda Husman, and J. F. Schijven, "Evaluation of water quality guidelines for public swimming ponds," *Environment International*, vol. 137, Article ID 105516, 2020.

[7] T. J. Gerken, M. C. Roberts, P. Dykema et al., "Environmental surveillance and characterization of antibiotic resistant *Staphylococcus aureus* at coastal beaches and rivers on the island of Hawai'i," *Antibiotics*, vol. 10, no. 8, Article ID 980, 2021.

[8] D. Thapaliya, E. J. Hellwig, J. Kadariya et al., "Prevalence and characterization of *Staphylococcus aureus* and methicillin-resistant *Staphylococcus aureus* on public recreational beaches in Northeast Ohio," *GeoHealth*, vol. 1, no. 10, pp. 320–332, 2017.

[9] H. Q. Raheem, L. H. Al-Ghazali, and F. A. Al-Marzook, "Antibacterial activity of copper oxide nanoparticles against methicillin resistant *Staphylococcus aureus* (MRSA)," *International Journal of Pharmaceutical Quality Assurance*, vol. 10, no. 3, pp. 138–141, 2019.

[10] T. Velempini, E. Prabakaran, and K. Pillay, "Recent developments in the use of metal oxides for photocatalytic degradation of pharmaceutical pollutants in water—a review," *Materials Today Chemistry*, vol. 19, Article ID 100380, 2021.

[11] S. M. Abu Nayem, S. S. Shah, S. B. Chaity et al., "Jute stick extract assisted hydrothermal synthesis of zinc oxide nanoflakes and their enhanced photocatalytic and antibacterial efficacy," *Arabian Journal of Chemistry*, vol. 15, no. 11, Article ID 104265, 2022.

[12] E. Baladi, F. Davar, and A. Hojjati-Najafabadi, "Synthesis and characterization of g–C_3N_4–$CoFe_2O_4$–ZnO magnetic nanocomposites for enhancing photocatalytic activity with visible light for degradation of penicillin G antibiotic," *Environmental Research*, vol. 215, Part 2, Article ID 114270, 2022.

[13] S. M. A. Nayem and M. Z. Hossain, "Enhanced photodegradation of methylene blue by Ag–ZnO nanocomposites," *Journal of Bangladesh Chemical Society*, vol. 33, pp. 57–60, 2021.

[14] M. Khairy and W. Zakaria, "Effect of metal-doping of TiO_2 nanoparticles on their photocatalytic activities toward removal of organic dyes," *Egyptian Journal of Petroleum*, vol. 23, no. 4, pp. 419–426, 2014.

[15] A. Hojjati-Najafabadi, M. Mansoorianfar, T. Liang et al., "Magnetic-MXene-based nanocomposites for water and wastewater treatment: a review," *Journal of Water Process Engineering*, vol. 47, Article ID 102696, 2022.

[16] A. Akhoondi, U. Feleni, B. Bethi, A. Olayiwola Idris, and A. Hojjati-Najafabadi, "Advances in metal-based vanadate compound photocatalysts: synthesis, properties and applications," *Synthesis and Sintering*, vol. 1, no. 3, pp. 151–168, 2021.

[17] G. Borkow, A. Felix, and J. Gabbay, "Copper-impregnated antimicrobial textiles; an innovative weapon to fight infection," in *Medical and Healthcare Textiles: Woodhead Publishing Series in Textiles*, S. C. Anand, J. F. Kennedy, M. Miraftab, and S. Rajendran, Eds., pp. 14–22, Cupron Inc, Greensboro, USA, 2010.

[18] S. Jillani, M. Jelani, N. U. Hassan, S. Ahmad, and M. Hafeez, "Characterization and biological studies of copper oxide nanostructures," *Materials Research Express*, vol. 5, no. 4, Article ID 045006, 2018.

[19] K. Saravanakumar, A. Sathiyaseelan, A. V. A. Mariadoss, H. Xiaowen, and M.-H. Wang, "Physical and bioactivities of biopolymeric films incorporated with cellulose, sodium alginate and copper oxide nanoparticles for food packaging application," *International Journal of Biological Macromolecules*, vol. 153, pp. 207–214, 2020.

[20] A. Bhaumik, A. Haque, P. Karnati, M. F. N. Taufique, R. Patel, and K. Ghosh, "Copper oxide based nanostructures for improved solar cell efficiency," *Thin Solid Films*, vol. 572, pp. 126–133, 2014.

[21] S. H. Gebre and M. G. Sendeku, "New frontiers in the biosynthesis of metal oxide nanoparticles and their environmental applications: an overview," *SN Applied Sciences*, vol. 1, Article ID 928, 2019.

[22] J. Singh, G. Kaur, and M. Rawat, "A brief review on synthesis and characterization of copper oxide nanoparticles and its applications," *Journal of Bioelectronics and Nanotechnology*, vol. 1, no. 1, Article ID 9, 2016.

[23] A. S. Lanje, S. J. Sharma, R. B. Pode, and R. S. Ningthoujam, "Synthesis and optical characterization of copper oxide nanoparticles," *Advances in Applied Science Research*, vol. 1, pp. 36–40, 2010.

[24] G. Sorekine, G. Anduwan, M. N. Waimbo et al., "Photocatalytic studies of copper oxide nanostructures for the degradation of methylene blue under visible light," *Journal of Molecular Structure*, vol. 1248, Article ID 131487, 2022.

[25] A. Muthuvel, M. Jothibas, and C. Manoharan, "Synthesis of copper oxide nanoparticles by chemical and biogenic methods: photocatalytic degradation and in vitro antioxidant activity," *Nanotechnology for Environmental Engineering*, vol. 5, Article ID 14, 2020.

[26] I. M. S. Araújo, R. R. Silva, G. Pacheco et al., "Hydrothermal synthesis of bacterial cellulose–copper oxide nanocomposites and evaluation of their antimicrobial activity," *Carbohydrate Polymers*, vol. 179, pp. 341–349, 2018.

[27] Z. N. Kayani, M. Umer, S. Riaz, and S. Naseem, "Characterization of copper oxide nanoparticles fabricated by the sol–gel method," *Journal of Electronic Materials*, vol. 44, pp. 3704–3709, 2015.

[28] Y. Zheng, L. Fu, F. Han et al., "Green biosynthesis and characterization of zinc oxide nanoparticles using *Corymbia citriodora* leaf extract and their photocatalytic activity," *Green Chemistry Letters and Reviews*, vol. 8, no. 2, pp. 59–63, 2015.

[29] M. Yang, J. He, M. Hu, X. Hu, C. Yan, and Z. Cheng, "Synthesis of copper oxide nanoparticles and their sensing property to hydrogen cyanide under varied humidity conditions," *Sensors and Actuators B: Chemical*, vol. 213, pp. 59–64, 2015.

[30] A. A. Menazea and M. K. Ahmed, "Silver and copper oxide nanoparticles-decorated graphene oxide via pulsed laser ablation technique: preparation, characterization, and photoactivated antibacterial activity," *Nano-Structures & Nano-Objects*, vol. 22, Article ID 100464, 2020.

[31] I. Z. Luna, L. N. Hilary, A. M. S. Chowdhury, M. A. Gafur, N. Khan, and R. A. Khan, "Preparation and characterization of copper oxide nanoparticles synthesized via chemical precipitation method," *Open Access Library Journal*, vol. 2, Article ID e1409, 2015.

[32] L. T. Shwe and P. P. Win, "Preparation of CuO nanoparticles by precipitation method," in *International Workshop on Nanotechnology*, pp. 1–5, Serpong, Indonesia, 2013.

[33] A. Singh, N. B. Singh, I. Hussain, H. Singh, and V. Yadav, "Synthesis and characterization of copper oxide nanoparticles and its impact on germination of *Vigna radiata* (L.) R. Wilczek," *Tropical Plant Research*, vol. 4, no. 2, pp. 246–253, 2017.

[34] S. M. A. Nayem, S. S. Shah, S. B. Chaity et al., "Jute stick extract assisted hydrothermal synthesis of zinc oxide nanoflakes and their enhanced photocatalytic and antibacterial efficacy," *Arabian Journal of Chemistry*, vol. 15, no. 11, Article ID 104265, 2022.

[35] A. L. Barry, F. Garcia, and L. D. Thrupp, "An improved single-disk method for testing the antibiotic susceptibility of rapidly-growing pathogens," *American Journal of Clinical Pathology*, vol. 53, no. 2, pp. 149–158, 1970.

[36] H. R. Ghorbani, I. Fazeli, and A. A. Fallahi, "Biosynthesis of copper oxide nanoparticles using extract of *E. coli*," *Oriental Journal of Chemistry*, vol. 31, no. 1, pp. 515–517, 2015.

[37] G. Manjari, S. Saran, T. Arun, A. Vijaya Bhaskara Rao, and S. P. Devipriya, "Catalytic and recyclability properties of phytogenic copper oxide nanoparticles derived from *Aglaia elaeagnoidea* flower extract," *Journal of Saudi Chemical Society*, vol. 21, no. 5, pp. 610–618, 2017.

[38] S. Sagadevan, K. Pal, and Z. Z. Chowdhury, "Fabrication of CuO nanoparticles for structural, optical and dielectric analysis using chemical precipitation method," *Journal of Materials Science: Materials in Electronics*, vol. 28, pp. 12591–12597, 2017.

[39] D. P. Volanti, D. Keyson, L. S. Cavalcante et al., "Synthesis and characterization of CuO flower-nanostructure processing by a domestic hydrothermal microwave," *Journal of Alloys and Compounds*, vol. 459, no. 1-2, pp. 537–542, 2008.

[40] M. Z. Hossain, S. Halder, A. N. Ahmed, and M. A. Gafur, "Synthesis of spherical silver nanoparticles by chemical reduction method," *Journal of Bangladesh Chemical Society*, vol. 30, no. 2, pp. 42–47, 2018.

[41] K. V. Yatish, R. Mithun Prakash, C. Ningaraju, M. Sakar, R. Geetha Balakrishna, and H. S. Lalithamba, "*Terminalia chebula* as a novel green source for the synthesis of copper oxide nanoparticles and as feedstock for biodiesel production and its application on diesel engine," *Energy*, vol. 215, Part B, Article ID 119165, 2021.

[42] M. Guzman, M. Arcos, J. Dille, S. Godet, and C. Rousse, "Effect of the concentration of $NaBH_4$ and N_2H_4 as reductant agent on the synthesis of copper oxide nanoparticles and its potential antimicrobial applications," *Nano Biomedicine and Engineering*, vol. 10, no. 4, pp. 392–405, 2018.

[43] P. Kumar, A. G. Nene, S. Punia et al., "Synthesis, characterization and antibacterial activity of Cuo nanoparticles," *International Journal of Applied Pharmaceutics*, vol. 12, no. 1, pp. 17–20, 2020.

[44] A. Raizada, D. Ganguly, M. M. Mankad, R. H. Krishna, and B. M. Nagabhushana, "A highly efficient copper oxide nanopowder for adsorption of methylene blue dye from aqueous medium," *Journal of Chemical Engineering Research*, vol. 2, no. 1, pp. 249–258, 2014.

[45] G. K. Weldegebrieal, "Photocatalytic and antibacterial activityof CuO nanoparticles biosynthesized using *Verbascum thapsus* leaves extract," *Optik*, vol. 204, Article ID 164230, 2020.

[46] R. Katwal, H. Kaur, G. Sharma, M. Naushad, and D. Pathania, "Electrochemical synthesized copper oxide nanoparticles for enhanced photocatalytic and antimicrobial activity," *Journal of Industrial and Engineering Chemistry*, vol. 31, pp. 173–184, 2015.

[47] A. George, D. Magimai Antoni Raj, X. Venci et al., "Photocatalytic effect of CuO nanoparticles flower-like 3D nanostructures under visible light irradiation with the degradation of methylene blue (MB) dye for environmental application," *Environmental Research*, vol. 203, Article ID 111880, 2022.

[48] J. Akter, K. P. Sapkota, M. A. Hanif, M. A. Islam, H. G. Abbas, and J. R. Hahn, "Kinetically controlled selective synthesis of Cu_2O and CuO nanoparticles toward enhanced degradation of methylene blue using ultraviolet and sun light," *Materials Science in Semiconductor Processing*, vol. 123, Article ID 105570, 2021.

[49] M. P. Rao, S. Anandan, S. Suresh, A. M. Asiri, and J. J. Wu, "Surfactant assisted synthesis of copper oxide nanoparticles for photocatalytic degradation of methylene blue in the presence of visible light," *Energy and Environment Focus*, vol. 4, no. 3, pp. 250–255, 2015.

[50] R. Sankar, P. Manikandan, V. Malarvizhi, T. Fathima, K. S. Shivashangari, and V. Ravikumar, "Green synthesis of colloidal copper oxide nanoparticles using *Carica papaya* and its application in photocatalytic dye degradation," *Spectrochimica Acta Part A: Molecular and Biomolecular Spectroscopy*, vol. 121, pp. 746–750, 2014.

[51] K. Dulta, G. K. Ağçeli, P. Chauhan, R. Jasrotia, P. K. Chauhan, and J. O. Ighalo, "Multifunctional CuO nanoparticles with enhanced photocatalytic dye degradation and antibacterial activity," *Sustainable Environment Research*, vol. 32, Article ID 2, 2022.

[52] S. Shirsat, D. Pawar, N. Jain, J. Pawar, V. S. Tale, and R. Henry, "Synthesis of copper oxide nanoparticles by chemical precipitation method for the determination of antibacterial efficacy against *Streptococcus* sp. and *Staphylococcus* sp." *Asian Journal of Pharmaceutical and Clinical Research*, vol. 12, no. 5, pp. 135–138, 2019.

[53] A. Azam, A. S. Ahmed, M. Oves, M. Khan, and A. Memic, "Size-dependent antimicrobial properties of CuO nanoparticles against Gram-positive and -negative bacterial strains," *International Journal of Nanomedicine*, vol. 7, pp. 3527–3535, 2012.

[54] S. Prakash, N. Elavarasan, A. Venkatesan, K. Subashini, M. Sowndharya, and V. Sujatha, "Green synthesis of copper oxide nanoparticles and its effective applications in biginelli reaction, BTB photodegradation and antibacterial activity," *Advanced Powder Technology*, vol. 29, no. 12, pp. 3315–3326, 2018.